ELSEVIER

Journal of Biomechanics 34 (2001) 1375–1386

JOURNAL OF BIOMECHANICS

www.elsevier.com/locate/jbiomech
www.JBiomech.com

# A model for strain amplification in the actin cytoskeleton of osteocytes due to fluid drag on pericellular matrix

Lidan You[a], Stephen C. Cowin[a], Mitchell B. Schaffler[b], Sheldon Weinbaum[a,*]

[a] *Department of Mechanical Engineering, The Center for Biomedical Engineering, City College of New York, The City University of New York, Convent Avenue at 140th Street, New York, NY 10031, USA*

[b] *Department of Orthopaedics, The Mount Sinai School of Medicine, One Gustave L. Levy Place, New York, NY 10029, USA*

Accepted 22 July 2000

**Abstract**

A model is presented that provides a resolution to a fundamental paradox in bone physiology, namely, that the strains applied to whole bone (i.e., tissue level strains) are much smaller (0.04–0.3 percent) than the strains (1–10 percent) that are necessary to cause bone signaling in deformed cell cultures (Rubin and Lanyon, J. Bone Joint Surg. 66A (1984) 397–410; Fritton et al., J. Biomech. 33 (2000) 317–325). The effect of fluid drag forces on the pericellular matrix (PM), its coupling to the intracellular actin cytoskeleton (IAC) and the strain amplification that results from this coupling are examined for the first time. The model leads to two predictions, which could fundamentally change existing views. First, for the loading range 1–20 MPa and frequency range 1–20 Hz, it is, indeed, possible to produce cellular level strains in bone that are up to 100 fold greater than normal tissue level strains (0.04–0.3 percent). Thus, the strain in the cell process membrane due to the loading can be of the same order as the in vitro strains measured in cell culture studies where intracellular biochemical responses are observed for cells on stretched elastic substrates. Second, it demonstrates that in any cellular system, where cells are subject to fluid flow and tethered to more rigid supporting structures, the tensile forces on the cell due to the drag forces on the tethering fibers may be many times greater than the fluid shear force on the cell membrane. 

*Keywords:* Osteocyte process; Shear stress; Drag force; Actin filament bundle; Strain amplification

## 1. Introduction

Bone is a dynamic system that can adjust its structure to its mechanical loading. The customary strains in whole bone in vivo are typically in the range of 0.04–0.3 percent for animal and human locomotion, but seldom exceed 0.1 percent (Rubin and Lanyon, 1984; Fritton et al., 2000). Osteocytes (Fig. 1) are believed to be the critical mechanical sensor cells (Cowin et al., 1991; Burger and Klein-Nulend, 1999), although the mechanism by which osteocytes perceive mechanical load is not known. One widely held idea is that cell membrane stretch occurs as a direct result of surrounding tissue deformation. If this is the case, then strain on osteocyte membranes should be comparable to the bone tissue strain. However, in vitro studies show that in order to induce any cellular response by direct mechanical deformation of bone cells, deformations need to be one to two orders of magnitude larger than the bone tissue strains normally experienced by the whole bone in vivo (Burger and Veldhuijzen, 1993; You et al., 2000). Similar cell strain magnitudes are needed to activate fibroblasts and chondrocytes ($\sim$15 percent) (Almekinders et al., 1993; Guilak et al., 1995), suggesting that in their sensitivity to mechanical strain, osteocytes may not be different from other connective tissue cells. However, in bone the larger strains needed to stimulate osteocytes cannot be derived directly from matrix deformations, as they would cause bone fracture. Thus, in bone there is an inherent contradiction between material and biological stimulation requirements. We present here an hypothesis and model to deal with this contradiction.

We consider first the flow of bone fluid due to mechanical loading. Between the osteocyte cell process

*Corresponding author. Tel.: +1-212-650-5202; fax: +1-212-650-6727.

*E-mail address:* weinbaum@me-mail.engr.ccny.cuny.edu (S. Weinbaum).

0021-9290/01/$ - see front matter 
PII: S0021-9290(01)00107-5

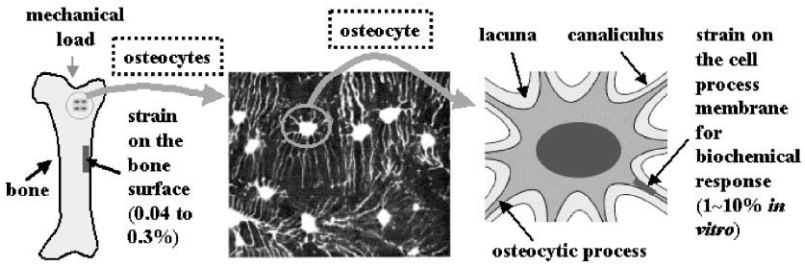


Fig. 1. This figure illustrates the paradox addressed in this paper. (a) An illustration of the small strains that the whole bone experiences, strains that are in the range 0.04 to 0.3 percent and seldom exceed 0.1 percent. The last two panels, (b) Photomicrograph of osteocytes encased in bone matrix (c) Osteocyte in lacuna, illustrate that large stains (1 to 10 percent) on cell membrane are needed to induce biochemical intracellular response in vitro. The paradox in the bone mechanosensing system is that the strains that activate the bone cells are two orders of magnitude larger than the strains to which the whole bone organ is subjected.

membrane and canalicular wall is the pericellular space through which the bone fluid flows. A pericellular organic matrix appears to fill the space (Sauren et al., 1992; Aarden et al., 1996). This matrix is supported by transverse fibrils (Shapiro et al., 1995) which appear to anchor and center the cell process in its canaliculus. When a whole bone is deformed, the deformation-induced pressure gradient will cause bone fluid to flow in the pericellular space of the lacunar-canalicular system (Piekarski and Munro, 1977; Weinbaum et al., 1994; Cowin, 1999; Knothe Tate and Knothe, 2000) and induce a drag force on the matrix fibers.

As proposed in Weinbaum et al. (1994) the fluid flow will also induce shear stress on the cell process membrane. These stresses have been shown to mechanically stimulate bone cells (Reich and Frangos, 1991; Williams et al., 1994). We thus ask which mechanical signal is more important in stimulating osteocytes? If the drag force on the matrix is the larger of the two forces, can it lead to an amplification of the whole bone strain at the cellular level?

Our model leads to two remarkable predictions. First, given an attached pericellular matrix (PM), the fluid drag force on the PM per unit length of cell process will be shown to be more than an order of magnitude larger than the fluid shearing force on the process membrane per unit length. Second, the fluid drag on an attached PM can lead to circumferential (hoop) strains in the membrane-cytoskeleton of the cell process which are up to two orders of magnitude greater than the strains in the mineralized bone matrix.

## 2. Model development

Our idealized model for an individual canaliculus with its central cell process (Fig. 2) is a tube containing a centrally positioned osteocyte process and its surrounding fluid annulus filled with a mesh-like PM.

### 2.1. The PM around the osteocyte process

For the pericellular component, only two structural elements are critical for this mechanical model: 1) a space filling PM with a fiber spacing $\Delta$ that is sufficiently small, and 2) transverse fibrils which tether the cell process to the canalicular wall. From a mechanics point of view, any matrix, which has these two characteristics, should function equivalently, although the degree of strain amplification will change with the fiber spacing $\Delta$. There is growing evidence to support this basic structure. First, a space filling PM surrounding osteocytes is well-established (Wassermann and Yaeger, 1965; Sauren et al., 1992; Shapiro et al., 1995; and Aarden et al., 1996). Second, transverse tethering elements were first clearly identified in Fig. 3 in Shapiro et al. (1995) and also observed in our own recent EM studies. The pericellular space surrounding the osteocyte process varies from 14 to 100 nm (Cooper et al., 1966; Weinger and Holtrop, 1974; King and Holtrop, 1975), depending on species, age, age of osteocyte, histological bone type, skeletal location etc. Our own EM studies on adult mice indicate a pericellular space of 30–50 nm. We also observed that the cell process is invariably located at the center of the canalicular cross-section suggesting that the transverse fibrils are tension elements that anchor and position the cell process within the canaliculus.

Both albumin and proteoglycan exist in the pericellular space (Owan and Triffitt, 1976; Sauren et al., 1992). The effective diameter of albumin is $\sim 7$ nm, similar to the spacing of glycosaminoglycans (GAG) side chains along a proteoglycan monomer (Buckwalter and Rosenberg, 1982). In our previous studies (Weinbaum et al., 1994; Cowin et al., 1995), Weinbaum and Cowin showed that this value of pore size leads to shear stresses of 0.5 to 3.0 Pa for mechanical loads in the physiological range and good agreement with the experimental data for the relaxation time of stress generated potentials (SGP) in

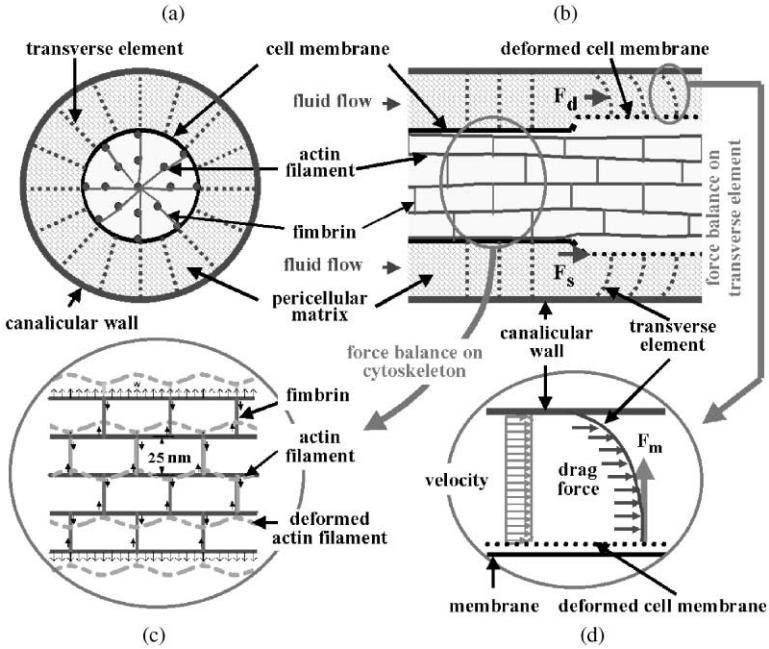


Fig. 2. Schematic model showing the structure of the PM, the IAC inside the process and the connection between the PM and the IAC. (a) Transverse cross-section of canaliculus showing the fluid annular shape of the region and transverse (radial) pericellular fibers. (b) Longitudinal cross-section before and after the transverse elements are deformed by the flow. (c) Schematic of the cell process cytoskeletal structure in longitudinal axial section used to estimate the Young's modulus in the radial (vertical) direction. Since the length of the cell process is 300 times its radius, it is considered infinite in the longitudinal (horizontal) direction. The axial actin filaments shown are modeled as continuous infinite beams with two types of loadings depending on whether the actin filaments are peripheral or interior. The small vertical arrows indicate the direction of the loading. The (fimbrin) links between these infinitely long beams are considered to be rigid. (d) Force balance on a transverse element.

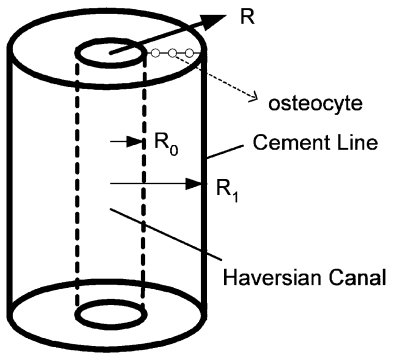


Fig. 3. Idealized model of an osteonal unit.

bone under four point bending (Salzstein and Pollack, 1987; Scott and Korostoff, 1990). Thus, in the present work, we assume a PM with a most likely pore size of 7 nm.

Finally, the matrix must be attached to the cell process and the canalicular wall in order for the drag force to be transmitted to the membrane and its underlying intracellular actin cytoskeleton (IAC). If such linker molecules are present, drag forces exerted on the matrix fibers will produce a tensile stress on these linker molecules which, in turn, will produce radial (hoop) strain in the IAC as schematically shown in Fig. 2. Possible candidates for these attachment molecules are CD44, laminin, and various integrins. (Gohel et al., 1995; Nakamura, 1995).

### 2.2. Structure of cell process IAC

Osteocyte processes contain a space filling actin bundle (King and Holtrop, 1975; Tanaka-Kamioka et al., 1998), whose actin filaments are cross-linked at regular intervals along the axis of the process by a linker molecule recently identified as fimbrin (Tanaka-Kamioka et al., 1998) as shown in Fig. 2c. The axial actin filaments are $\sim$6 nm in diameter. Fimbrin is also found in intestinal microvilli (Glenney et al., 1981) as well as non-intestinal cell microvilli (Bretscher and Weber, 1980). The typical spacing of fimbrin cross-linked actin filaments in microvilli is $\sim$25 nm (Chailley et al., 1989). This spacing is consistent with the EM observation in King and Holtrop (1975) and Tanaka-Kamioka et al. (1998) for an osteocyte process.

## 3. Mathematical formulation

### 3.1. The drag force on the fibers

The solution for the fluid flow in the fiber filled fluid annulus surrounding the cell process is described in

Weinbaum et al. (1994). This solution can be used to determine the integrated shear force $F_s$ (Fig. 2b) on the entire cell process membrane,

$$F_s = 2\pi aL\tau_w = 2\pi aL\left(\mu\frac{\partial u}{\partial \rho}\right) = 2\pi aL\left(\frac{b}{\gamma}\right)\frac{\partial p}{\partial R}\left[A_1 I_1\left(\frac{\gamma}{q}\right) - B_1 K_1\left(\frac{\gamma}{q}\right)\right]. \quad (1)$$

Here $a$ is the radius of the osteocytic process, $L$ is the length of the cell process, $\mu$ is the fluid viscosity, $R$ is the radial coordinate in the osteon (Fig. 3), or the axial coordinate in the canaliculus, $\rho$ is the radial coordinate in the canaliculus, $p$ is the fluid pressure, $b$ is the radius of the canalicular wall, and $\tau_w$ is the fluid shear stress on the osteocyte process membrane. The coefficients $A_1$, $B_1$, and parameters $\gamma$ and $q$ are given in Weinbaum et al. (1994). $I_1$ and $K_1$ are modified Bessel functions of first order. The radial pressure gradient $\partial p/\partial R$ along the axis of the fluid annulus is based on the theory in Zeng et al. (1994) for flow in an osteon due to axial loading.

The permeability constant, $k_p$, used to calculate $\tau_w$ here depends on the spacing of the tranverse elements (core proteins) and the GAG side chains along these core proteins. The fiber spacing $\Delta$ is the primary determinant of $k_p$. A simple expression for $k_p$ is derived in Appendix A, which can be found on the J. Biomech. WEB site.

The total drag force (Fig. 2b) exerted on the transverse elements between the canalicular wall and the cell process membrane can be obtained by integrating the distributed force, the first term on the left hand side of Eq. (2) in Weinbaum et al. (1994), over the fluid annulus

$$F_d = 2\pi\left[\int_a^b \rho\left(\frac{\mu}{k_p}u\right)\mathrm{d}\rho\right]L = 2\pi L\frac{\partial p}{\partial R}\left\{\frac{b^2}{\gamma}[A_1 I_1(\gamma) - B_1 K_1(\gamma)] - \frac{b^2}{\gamma q}\left[A_1 I_1\left(\frac{\gamma}{q}\right) - B_1 K_1\left(\frac{\gamma}{q}\right)\right] - \frac{b^2 - a^2}{2}\right\} \quad (2)$$

From Eqs. (1) and (2) the force ratio $F_d/F_s$ is given by

$$F_r = F_d/F_s = \frac{2q^2[A_1 I_1(\gamma) - B_1 K_1(\gamma)] - \gamma q(q^2 - 1)}{A_1 I_1(\gamma/q) - B_1 K_1(\gamma/q)} - 1. \quad (3)$$

Note $F_r$ depends only on the canalicular and fiber geometry and is independent of $\partial p/\partial R$.

### 3.2. Flow-induced strain in the IAC

We next wish to derive a constitutive relation coupling the deformation of the transverse fibrils in the PM and the IAC. In our idealized model sketched in Fig. 2d the transverse elements are treated as inextensible but flexible tensile fibers whose load is transduced across the cell process membrane to its IAC whose effective Young's Modulus is $E^*$.

#### 3.2.1. Force balance on IAC

The constitutive equation for the actin cytoskeleton in the cell process is:

$$\sigma_\rho = E^*\varepsilon_\rho, \quad (4)$$

where $\sigma_\rho$ is the radial stress in the actin cytoskeleton and $\varepsilon_\rho$ is its radial strain.

Although there is extensive literature for determining $E^*$, these studies, e.g., Satcher and Dewey (1996), Shin and Athanasiou (1999), describe the modulus for the 3-D actin network in the main cell body but not cytoplasmic protrusions, such as microvilli and cell processes. The one exception is the recent model of Guo et al. (2000) for the brush border microvilli. Therefore, we have developed, from first principles, a new basic model for the osteocytic cell processes based on the ultrastructure observed in King and Holtrop (1975) and Tanaka-Kamioka et al. (1998), see Fig. 2c. This model for determining $E^*$ is briefly summarized in Appendix B, which can be found on the J. Biomech. WEB site.

The final expression for $E^*$, Eq. (B.5), is

$$E^* = \frac{203EI}{l_2^4}, \quad (5)$$

where $EI$ is the flexural rigidity of an individual actin filament and $l_2$ is the spacing of the cross-links. Three studies, Oosawa (1977), Kishino and Yanagida (1988) and Dupuis et al. (1997) using different experimental techniques indicate that $EI \sim 1.5\times10^{-26}\,\mathrm{Nm}^2$. Therefore,

$$E^* = 487.2\,\mathrm{kPa}. \quad (6)$$

One notes that this value of $E^*$ is two orders of magnitude larger than the measured value for the osteoblastic cell body, 2.5 kPa, measured in Shin and Athanasiou (1999). This difference will be discussed later.

#### 3.2.2. Interaction between PM and IAC

The radial force balance on the cell process cytoskeleton in Fig. 4 is given by

$$P_{equ.} = \sigma_\rho, \quad (7)$$

where $P_{equ.}$ is the equivalent pressure induced by the tension bearing transverse elements in the PM:

$$P_{equ.} = T_x/\Delta_1^2. \quad (8)$$

Here $\Delta_1$ is the distance between the transverse elements, $T_x$ is the tensile force exerted by each element and $\Delta_1^2$ is its associated membrane area. From Eqs. (4), (7) and (8)

$$T_x = \Delta_1^2 P_{equ.} = \Delta_1^2 E^*\varepsilon_\rho. \quad (9)$$

The circumferential hoop strain in the cell process membrane (the change in length per unit original length of

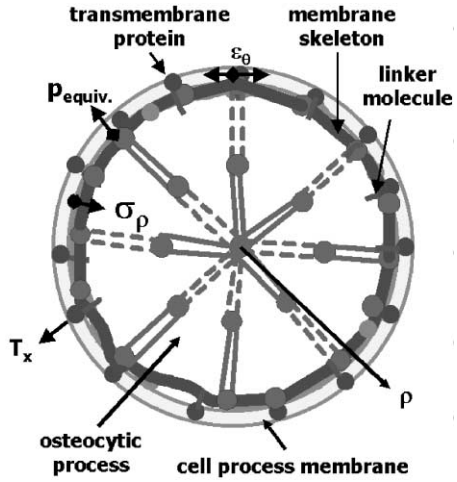


Fig. 4. Idealized model showing the force balance on the cell process membrane skeleton in transverse section.

the process membrane in the hoop direction) is given by

$$\varepsilon_\theta = \lambda_\theta - 1 = (\rho_1/\rho_0) - 1 = \varepsilon_\rho, \tag{10}$$

where $\rho_1$ and $\rho_0$ are the radii of the stretched and unstretched membrane, respectively.

*3.2.3. Force balance on the transverse elements*

Due to the high fiber density, the flow in the fluid annulus is a plug flow except for the thin fiber interaction layers that are of order $\Delta/2$ near the boundaries of the fluid annulus. Thus, the drag force exerted on the load bearing fibers in the axial direction can be treated as uniform.

In view of this uniform loading, the equilibrium shape of the transverse element is the well-known catenary equation

$$\frac{w_f s}{T_x} = \sinh\left(\frac{w_f d}{T_x}\right), \tag{11}$$

where $d$ is the distance between the canalicular wall and cell process membrane. In the present application $T_x$ is the constant radial component of the force exerted by one transverse element on the IAC and $w_f$ is the drag force per unit length on each transverse element. The drag on each transverse element $sw_f$ is obtained by dividing the total drag force on all the transverse elements in the annulus, $F_d$, by the total number of tensile elements, $2\pi\rho_0 L/\Delta_1^2$, attached to the membrane surface

$$sw_f = F_d/\left(2\pi\rho_0 L/\Delta_1^2\right), \tag{12}$$

where $s$ is the total length of the transverse element.

*3.2.4. Strain on the process membrane*

Substituting Eqs. (1) and (3) into Eq. (12) , we have

$$sw_f = \frac{F_r\tau_w a\Delta_1^2}{\rho_0} = \frac{F_r\tau_w\rho_1\Delta_1^2}{\rho_0}. \tag{13}$$

Note that $\tau_w$ is evaluated from Eq. (28) in Zeng et al. (1994) with $a = \rho_1$, and $F_d$ in Eq. (12) includes the drag on all the GAG side chains, which can be considered as a distributed force on each transverse element.

From the geometry in Fig. 2, the strain $\varepsilon_\theta$ in Eq. (10) is given by

$$\varepsilon_\theta = \frac{s-d}{\rho_0}. \tag{14}$$

Substituting Eqs. (9), (10), (13) and (14) into Eq. (11) one obtains

$$\beta\frac{(1+\varepsilon_\theta)}{\varepsilon_\theta} = \sinh\left[\beta\frac{(1+\varepsilon_\theta)}{\varepsilon_\theta}\left(1-\frac{\rho_0\varepsilon_\theta}{s}\right)\right], \tag{15}$$

or

$$\beta\frac{(1+\varepsilon_\theta)}{\varepsilon_\theta} = \sinh\left[\beta\frac{(1+\varepsilon_\theta)}{\varepsilon_\theta}\left(1-\frac{\varepsilon_\theta}{q-1}\right)\right], \tag{16}$$

where

$$\beta = \frac{F_r\tau_w}{E^*} = \frac{F_d}{2\pi\rho_0 LE^*} = \frac{F_d/A}{E^*} = \frac{f_d}{E^*}. \tag{17}$$

Here $A$ is the total area of the process membrane, and $f_d$ is the drag force on the fibers per unit area of the cell process membrane. Therefore, $\beta$ is a new fundamental dimensionless parameter, which relates the drag force on the fibers to the elastic properties of the IAC.

In Cowin et al. (1995), it was shown that close agreement with experiment could be obtained for both the phase and magnitude of the stress generated potential when $q$ was approximately 2. For $q = 2$, $\rho_0 = s = a = b/2$ and Eq. (16) reduces to

$$\beta\frac{(1+\varepsilon_\theta)}{\varepsilon_\theta} = \sinh\left[\beta\frac{(1+\varepsilon_\theta)(1-\varepsilon_\theta)}{\varepsilon_\theta}\right]. \tag{18}$$

Eq. (16), or its simplified form, Eq. (18), is the basic dimensionless relationship between the hoop strain $\varepsilon_\theta$ on the cell process membrane and the dimensionless fluid dynamic loading parameter $\beta$.

Finally, the strain amplification ratio $\varepsilon_r$ is defined as

$$\varepsilon_r = \frac{\varepsilon_\theta}{\varepsilon_b}, \tag{19}$$

where $\varepsilon_b$ is the strain on the bone surface,

$$\varepsilon_b = \sigma_b/E_b, \tag{20}$$

$\sigma_b$ is the mechanical load on the whole bone and $E_b$ is its Young's Modulus.

## 4. Parameter values

The values of the parameters $a_0$, $q$, $\mu$, $l$ and $\Delta$ are discussed in detail in Weinbaum et al. (1994), Zeng et al. (1994) and Cowin et al. (1995). It is estimated in the literature that $a$ is typically 50 nm (Cooper et al., 1966; Marotti et al., 1990; note that these references suggest a range of values depending on species, age, histological

bone type, and skeletal location). In our study, we have chosen $a = 50$ nm. The radius $a_0$ of the GAG side chains is 0.6 nm (Curry, 1986) and their most likely spacing $\Delta$ along the core protein is 7 nm. The length of the GAG is 20 nm and the spacing of the transverse elements is taken to be twice this value, 40 nm, so that the extended GAG forms a space filling arrangement. The predicted values of $q$ fall within the range $1.5 \leqslant q \leqslant 3.0$, observed in morphometric studies. In the present work, if not specified, we assume $q = 2.0$, and hence the nominal width of the fluid annulus, $b - a = 50$ nm. We also investigate the role of $q$ by looking at the changes of the force ratio, $F_r$, and hence the dimensionless parameter $\beta$, when $q$ is changed. The viscosity $\mu$ of the fluid in the annulus is $10^{-2}$ dyn/cm$^2$, the value of water.

## 5. Results

In Fig. 5 we have plotted our solution for the force ratio, $F_r = F_d/F_s$, as a function of the GAG spacing $\Delta$. As shown in Eq. (3), $F_r$ is independent of the magnitude and frequency of the mechanical loading and thus an intrinsic property of the matrix and canaliculus geometry. The important result discovered in plotting $F_r$ against $\Delta$ was that $F_r \gg 1$ over the entire physiological range of $\Delta$ ($5 \sim 12$ nm). For $\Delta = 7$ nm, the most likely value of $\Delta$, the drag force is *19.6* times larger than the shear force per unit length of cell process. As the fiber spacing increases, the relative importance of the drag force will decrease markedly, and when the fiber spacing $\Delta = 39$ nm, a non-physiological value, $F_d/F_s$ will be approximately unity.

The effect of frequency on the strain amplification ratio and the absolute strain at different loading magnitudes are shown in Fig. 6, where $\varepsilon_r$, given by

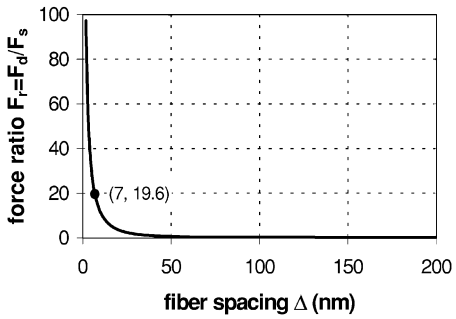


Fig. 5. The relationship between force ratio $F_r$ and average fiber spacing $\Delta$. Note the force ratio at $\Delta = 7$ nm is 19.6. $\Delta = 7$ nm is typical of the average spacing of GAG side chains along a core protein and the effective diameter of the albumin molecule which is known to be sieved by an equivalent matrix in capillary endothelium. This varies between 5 and 12 nm. The force ratio $F_r$ is defined as the ratio of the drag force on the fibers to the shear force on the cell process membrane per unit length of cell process.

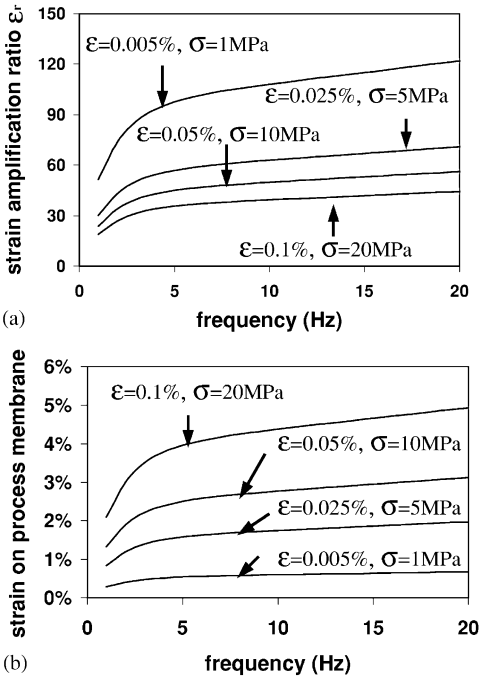


Fig. 6. Strain amplification. (a) Plot of the strain amplification ratio $\varepsilon_r$ as a function of the load frequency for different load magnitudes. Strain amplification ratio is defined as the ratio of the hoop strain in the cell process membrane to the bone surface strain at the osteonal lumen. $\varepsilon$ is the strain on the whole bone; $\sigma$ is the load on the whole bone. (b) Plot of the cell process membrane strain $\varepsilon_\theta$ as a function of the load frequency for different load magnitudes. $\varepsilon$ is the strain on the whole bone; $\sigma$ is the load on the whole bone.

Eq. (19), and $\varepsilon_\theta$, given by Eq. (14), are both plotted against the loading frequency from 1 to 20 Hz. The hoop strain is calculated at the position of maximum flow or pressure gradient, which is located at, $R = R_i$, the surface of the Haversian canal. Thus, the hoop strain and the strain amplification ratio shown in Figs. 6a and b can be considered as an upper bound. The curves show a monotonic increase in the amplification ratio as a function of frequency for a prescribed loading. One observes that the amplification ratio varies from 19 to 122 and depends significantly on the magnitude of the loading. When the loading magnitude is 1 MPa, corresponding to 50 μ strain at the osteonal lumen, $\varepsilon_r = 122$ at 20 Hz. For this loading the cell process strain is 0.68 percent. For a 20 MPa load at 20 Hz, $\varepsilon_r = 44$ and the cell process strain is 4.9 percent. The corresponding values of $\varepsilon_r$ at 1 Hz for a 1 and 20 MPa load are 51 and 19 and the corresponding strains are 0.29 and 2.1 percent, respectively. Strains of the order of 0.3 percent or greater fall in the range where cellular level biochemical responses have been observed in vitro in four point bending (Pitsillides et al., 1995).

Fig. 7 compares the strains on the process membrane using the measured value for $E^*$ for an osteoblast cell body, 2.5 kPa (Shin and Athanasiou, 1999), and the value for $E^*$, 487 kPa, predicted by our model for an

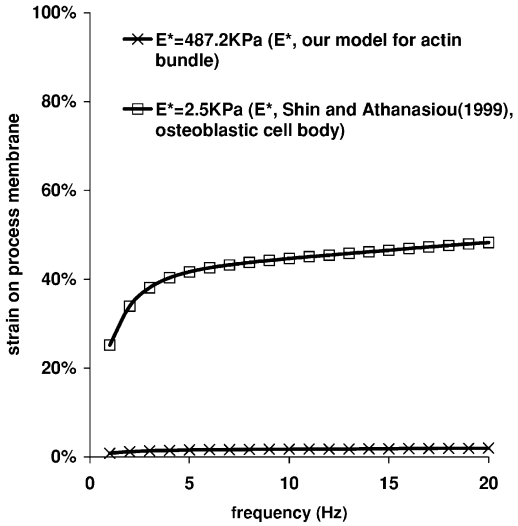


Fig. 7. The comparison of the strain on the osteocyte process membrane using the measured Young's modulus of osteoblastic cell body, $E^* = 2.5$ kPa (Shin and Athanasiou, 1999), and our predicted the Young's modulus of a closely packed actin filament bundle, $E^* = 487.2$ kPa. Both strains are calculated when the loading on bone is 5 MPa.

Table 1
Sensitivity of cytoskeletal hoop strain to model parameters[a]

| | | 1 Hz (%) | 2 Hz (%) | 5 Hz (%) | 10 Hz (%) | 20 Hz (%) |
|---|---|---|---|---|---|---|
| GAG spacing $\Delta$ (nm) | 5 | 1.26 | 1.58 | 1.82 | 2.06 | 2.47 |
| | 7 | 0.83 | 1.20 | 1.58 | 1.75 | 1.97 |
| | 12 | 0.37 | 0.59 | 0.99 | 1.31 | 1.51 |
| Fimbrin spacing $l_2$ (nm) | 25 | 0.13 | 0.19 | 0.25 | 0.28 | 0.31 |
| | 50 | 0.83 | 1.20 | 1.58 | 1.75 | 1.97 |
| | 100 | 5.23 | 7.47 | 9.78 | 10.8 | 12.1 |
| Width of pericellular space $b-a$ (nm) | 20 | 0.60 | 0.67 | 0.78 | 0.94 | 1.14 |
| | 50 | 0.83 | 1.20 | 1.58 | 1.75 | 1.97 |
| | 100 | 0.86 | 1.35 | 2.26 | 2.93 | 3.35 |

[a] Table of the predicted values of strains on the osteocyte process membrane obtained for different values of GAG spacing $\Delta$, fimbrin spacing $l_2$, and width of pericellular space $b-a$ when the loading on the whole bone is taken as 5 MPa.

actin filament bundle. For both cases, the loading on bone is taken as 5 MPa. One can see that using this measured value for the cell body will lead to unrealistically large cell process strains of 25–50 percent. In contrast, our calculation of $E^*$ for an actin filament bundle leads to strains of 1–2 percent, which are more reasonable. The large increase in the value of $E^*$ for the actin filament bundle is due to the tight packing of the actin filaments and the close spacing $l_2$ of the fimbrin cross-links. This will be discussed later in Table 1.

The relationship between the dimensionless loading parameter, $\beta$, and the strain on the cell process membrane, $\varepsilon_\theta$, defined by Eq. (14), is plotted in Fig. 8, for $\varepsilon_\theta$ in the range 0.3–8 percent and representative values of $q$ between 1.2 and 6. For the osteocyte process $q$ lies in the range of 1.5–3.0. One of the striking features in Fig. 6a is that the strain amplification ratio is a function of loading at a given frequency and decreases as the loading increases, whereas $\varepsilon_b$ increases linearly with loading. It is evident from Fig. 8 that $\varepsilon_\theta$ does not increase linearly with $\beta$ since Eq. (16) is nonlinear. It is much like pulling a string back on a bow and arrow. The initial deflection is easy and the force required to produce a large displacement increases non-linearly with the applied force.

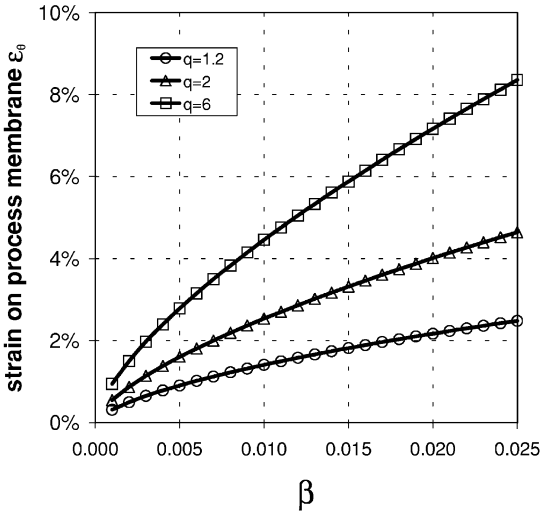


Fig. 8. The relationship between $\varepsilon_\theta$ and $\beta$ when $q = 1.2$, 2 or 6, see Eq. (16), where $\varepsilon_\theta$ is the hoop strain in the cell process membrane and $\beta$ is a dimensionless loading parameter, defined by $\beta = f_d/E^*$.

## 6. Discussion

The effect of fluid drag on PM and the resulting strain on the IAC of the cell process and its plasma membrane are examined for the first time using a combined hierarchical mechanical model. The new model suggests that the small mechanically induced strains on whole bone at physiological loading can be greatly amplified at the cell membrane level, if the fluid drag forces on the PM are transmitted to the IAC in the cell process. This amplification can lead to strains in a range where intracellular biochemical responses have been observed experimentally.

In the past, researchers examining the effect of fluid flow on cells had focused their attentions nearly exclusively on the response of cells to fluid shear stress. The drag force exerted on PM fibers has never been considered. However, one observes in Fig. 5, that at a GAG spacing of 7 nm, the fiber spacing where the matrix could serve as a molecular filter for albumin

(Weinbaum, 1998), and the typical spacing of GAG side chains along protein monomers (Buckwalter and Rosenberg, 1982), the force ratio $F_r$ would be $\sim 20$ in the fluid annulus. Furthermore, this ratio from Eq. (3) is independent of the value of the loading magnitude and loading frequency. This important result suggests that the drag force on the fibers could be the dominant stimulus for the cell's mechanosensory system, rather than, or in addition to the fluid shear stress on the cell process, as originally proposed in Weinbaum et al. (1994).

Experimental in vitro cell culture studies on elastic substrates have typically been performed at strain levels of 1–10 percent (Murray and Rushton, 1990; Burger and Veldhuijzen, 1993). Strain levels in four point bending are significantly lower, 0.38 percent (Pitsillides et al., 1995). However, the peak levels of the strain on whole bone tissue range from about 0.04–0.2 percent in humans under varied activities (Lanyon et al., 1975 and Burr et al., 1996) and 0.04–0.3 percent for animal locomotion (Fritton et al., 2000). Thus, the strain levels achieved in in vitro cell culture studies are much greater than the whole tissue strains experienced physiologically in vivo. Klein-Nulend et al., 1995 and You et al., 2000 have shown that when physiological strains of less than one percent are applied in cell culture, there is no observed cellular response. In contrast, Pitsillides et al. (1995) reported rapid increase in NO production at 0.38 percent strain for bone cells in four point bending. However, this load is at the extreme of physiological loading. These observations for bone cells have cast doubt on any previous theory that proposed that cell stretch could be one of the candidates for cell activation in bone.

The new strain amplification hypothesis and model in the present study predict that the strain induced on the whole bone can be amplified by a factor of 20 to 100 or more at the cell membrane level and produce maximum strains from 0.3 to nearly 5 percent on the cell process membrane for mechanical loading in the physiological range if the drag forces on the PM can be transmitted to the IAC of the cell process. Note also that, for low magnitude- high frequency loads, the amplification effect is significantly greater than for high magnitude-low frequency loads. Eqs. (15) or (16) and Fig. 8 show that the relation between the drag force on a fiber, $F_d/(2\pi\rho_0 l/\Delta_1^2)$, and the hoop strain, $\varepsilon_\theta$, on the process membrane is nonlinear. This could be a factor in explaining why Rubin and McLeod (1996) observed that low magnitude, high frequency mechanical loading appeared to be particularly effective in maintaining bone mass.

The analysis has brought to light a fundamental new dimensionless group, $\beta = f_d/E^*$, relating the drag force on the PM to the elastic modulus of the IAC. In Fig. 8, we have plotted the nonlinear relationship between $\beta$ and $\varepsilon_\theta$ when $\varepsilon_\theta$ is in the range 0.3 to 8 percent where one would anticipate an intracellular biochemical response to stretch. The form of Eqs. (15) and (16) is dictated by the deformed shape of the transverse fibrils in the PM which, in this case, is a catenary curve because the loading due to the fluid flow is uniform. A similar expression needs to be developed for an ellipsoidal geometry. This would be useful in describing the flow past the body of the osteocyte in its lacuna or the flow through the matrix surrounding a chondrocyte.

There are several simplifications in the model. We did not consider the change in shape of the fluid annulus or the change in permeability of the PM due to the fluid flow. This change is expected to be small since $\Delta$ will not change significantly and the changes in cell process diameter are at most a few percent, see Fig. 6b.

We have also treated the PM as a simple rectangular mesh in calculating $k_p$. However, one can show that the basic predictions will not change significantly for a random matrix. The key parameter in determining $k_p$ is $\Delta$. Hu et al. (2000) have shown that the surface glycocalyx on endothelial cells has sieving properties very close to 7 nm. Our calculation in Table 1 shows that if we vary $\Delta$ from 5 to 12 nm the strain on osteocyte process membrane will change by less than a factor of 4 for all frequencies above 1 Hz.

The IAC structure assumed for the cell process is based on numerous histological studies (Weinger and Holtrop, 1974; King and Holtrop, 1975; Holtrop, 1975, Shapiro et al., 1995; Tanaka-Kamioka et al., 1998). The two key parameters are the spacing of the actin filaments, $l_1$, and the distance between the fimbrin linker molecules, $l_2$. The variation of $l_1$ will not greatly change our final results since the strain is induced through bending rather than stretching of the axial actin filaments. $l_2$ is estimated to be $\sim 50$ nm based on the electromicrographs in Tanaka-Kamioka et al. (1998) and the fimbrin spacing in the actin bundles of microvilli. Distances larger than this will lead to greater strain amplification. EM studies indicate that $l_2$ should be larger than $l_1$ (Shapiro et al., 1995; Horwitz, 1997; Tanaka-Kamioka et al., 1998). $l_1$ has been taken as 25 nm. The calculations in Table 1 for $l_2 = 25$ nm and 100 nm indicate that $l_2$ is a critical parameter in predicting IAC strain. A doubling of $l_2$ leads to a six fold increase in cell process strain whereas the value of $E^*$ increases as $l_2^4$, see Eq. (5). In contrast, varying the width of the pericellular space, $b - a$, from 20 to 100 nm produces much smaller strain variations in the IAC, see Table 1.

An important insight in formulating the new hypothesis was the realization that the cytoskeleton of the osteocyte process closely resembles the actin filament bundles in the microvilli of the small intestine and proximal tubule (Maunsbach, 1973; Mooseker and Tilney, 1975; Tanaka-Kamioka et al., 1998). The structural rigidity of this actin filament bundle to

bending was examined for the first time in Guo et al. (2000) where it is shown that the brush border microvilli are relatively stiff structures that are well suited to serve as mechanotransducers. One of the crucial observations for the cell process is that it is invariably located at the center of the canalicular cross-section in electron micrographs. Since the cell process is relatively stiff and the canaliculi are seldom straight conduits, it is hard to imagine how such centering can be achieved without there being tensile supporting structures which tether the cell process and its cytoskeleton to the canalicular wall. This indirect evidence let the authors to hypothesize the existence of the transverse elements in the PM, before we were aware that such structures have already been identified in Shapiro et al. (1995). Our own recent electron microscopic studies have since confirmed this observation.

Although we have applied the model using pressure gradients calculated for an osteonal geometry, the bone geometry is secondary since the strain amplification mechanism applies at the canalicular level. While the PM is believed to contain proteoglycans (Sauren et al., 1992), this is also non-essential. There are other candidates for the PM, e.g., CD44 molecules with GAG side chains. CD44 has a terminus for hyaluronan, a major component of endothelial glycocalyx. The particular molecules involved are not important in a mechanical model. The results at the cellular level depend only on the canalicular geometry, the fiber spacing and the assumed model for the IAC.

## Acknowledgements

This research has been supported by NIH grants R01AR44211 and R01AR41210. This research has been performed in partial fulfillment of the requirements for the Ph.D. degree by L. You from the city university of New York.

## Appendix A. The calculation of the permeability $k_p$ in the pericellular space

If the GAG side chains form a rectangular lattice that radiates fore and aft and laterally about the core protein (proteoglycan) at intervals $\Delta$ along its length (see Fig. 2a and b), the total length of GAG associated with each core protein is $s/\Delta(4l_{GAG})$, where $s$ is the length of the core protein and $l_{GAG}$ is the length of the GAG side chains. Since we have assumed $\Delta = 7\,\text{nm}$ and $l_{GAG} = 20\,\text{nm}$, the length ratio between the GAG side chains and the core proteins, $r_1 = 4l_{GAG}/\Delta \gg 1$, which suggests that the length of the GAG far exceeds that of the core protein. The drag on the core protein is thus largely due to its GAG side chains which, for simplicity, are arranged either transverse or parallel to the flow with equal length. The weighted hydraulic resistance due to the GAG plus the core protein is thus given by

$$\frac{1}{k_p} = \frac{r_1}{r_1+1}\left(\frac{1}{2k_{p1}} + \frac{1}{2k_{p2}}\right) + \frac{1}{r_1+1}\left(\frac{1}{k_{p1}}\right), \tag{A.1}$$

where $k_{p1}$ is the Darcy permeability of the transverse fibers including the core proteins and $k_{p2}$ the axial fibers. The expression for $k_{p1}$ is given in Tsay and Weinbaum (*J. Fluid Mech.* 226, 125–148, 1991) as

$$k_{p1} = 0.0572a_0^2\left(\frac{\Delta}{a_0}\right)^{2.377}, \tag{A.2}$$

The expression for $k_{p2}$ is given in Cowin et al. (1995) as

$$k_{p2} = 0.147a_0^2\left(\frac{\Delta}{a_0}\right)^{2.285}. \tag{A.3}$$

## Appendix B. The method for estimating the Young's modulus of the cytoskeleton structure, $E^*$, in the radial direction

The purpose of this appendix is to describe the derivation associated with the estimate of 487.2 kPa for the Young's modulus of the cell process IAC. The derivation was illustrated in Fig. 2c in main body and Figs. 9 and 10 in this appendix. The longitudinal actin filaments are modeled as infinitely long continuous beams. The outer filaments beneath process membrane (Fig. 9b) have a continuously distributed load representing the load transmitted by the transverse elements in the PM, whereas the inner ones have point force loads, $P$, transmitted by the fimbrin cross-links (Fig. 9a). The (fimbrin) links between these infinitely long beams are considered to be rigid because the deflection of the actin filament, which is loaded transversely, will be much larger than the strain of the fimbrin linker molecules which are loaded axially. The radial deflection of the cell process cytoskeletal structure illustrated in Fig. 2c is $\bar{\delta} = \bar{\delta}_1 + 2\bar{\delta}_2 + \bar{\delta}_3$, where the $\bar{\delta}_i$, $i = 1, 2, 3$, are illustrated in Fig. 9. The bar is superimposed upon these deflections to indicate that they are average, or mean, deflections. The gage length over which the deflection occurs is $2l_1$, where $l_1$ is illustrated in Fig. 9, and the radial strain is given by $\varepsilon = \bar{\delta}/2l_1$. It follows from Hooke's law that this strain is related to the stress $\sigma$ by $E^* = \sigma/\varepsilon$, and it is the value of the Young's modulus $E^*$ that we seek in this calculation. The stress $\sigma$ may also be expressed in terms of quantities illustrated in Fig. 2c, namely the length $l_1$, the length $l_2$ and the distributed load $w$ per unit length: $\sigma = w \times l_2 \times 8/l_2 \times 2\pi \times 2l_1$. Combining these results to obtain an expression for $E^*$, we find that $E^*$ can expressed in terms of the three mean deflections and the known

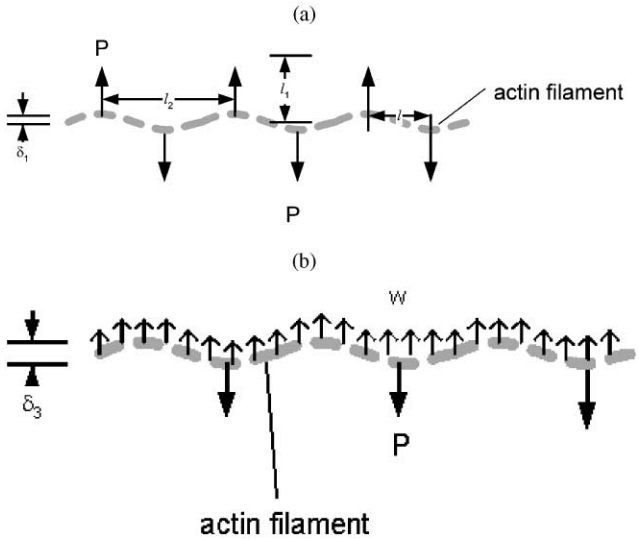


Fig. 9. Illustration of the longitudinal actin filaments modeled as continuous infinite beams with two types of loadings; the two types of loadings are illustrated in (a) and (b). (a) A typical longitudinal actin filament in the interior portion of the cell process cytoskeletal structure where the load is applied by the fimbrin cross-links in alternate directions in a staggered fashion. (b) This continuous infinite beam models an exterior longitudinal actin filament. It is loaded in one direction by the fimbrin cross-links and in the other direction by a continuously distributed load representing the applied external loading due to the extracellular matrix.

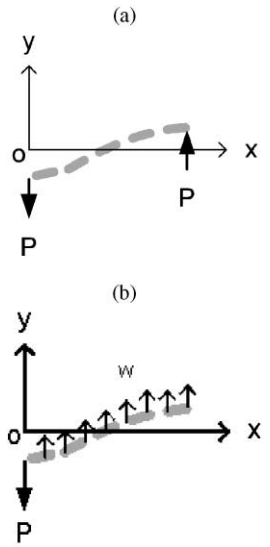


Fig. 10. Illustration of the unit length of the longitudinal actin filaments modeled as continuous infinite beams with the two types of loading, the two types of loading described in Fig. 9. (a) A typical longitudinal actin filament in the interior portion of the cell process cytoskeletal structure loaded by fimbrin links in alternate directions in a staggered fashion. (b) This continuous infinite beam models a peripheral longitudinal actin filament beneath the process membrane. It is loaded in one direction by the fimbrin cross-links and in the other direction by a continuously distributed load representing the applied external loading.

distributed loading $w$. Thus

$$E^* = \frac{4w/\pi}{\bar{\delta}_1 + 2\bar{\delta}_2 + \bar{\delta}_3}. \tag{B.1}$$

This result reduces the determination of $E^*$ to the determination of the three $\bar{\delta}_i$, $i = 1, 2, 3$. The determination of these quantities is described in the next paragraph.

The theory used for the determination of the three $\bar{\delta}_i$, $i = 1, 2, 3$, is classical beam theory. The fourth order differential equation governing the deflection $y$ of the a beam is given by

$$EI\frac{d^4y}{dx^4} = w, \tag{B.2}$$

where $E$ is the Young's modulus of the beam material, $I$ is the area moment of inertia of the cross-sectional area about a centroidal axis, $w(x)$ is the distributed load along the beam and $x$ is the coordinate running along the longitudinal axis of the beam. The product $EI$ is the flexural rigidity. We apply Eq. (B.2) and the associated theory to the continuous infinite beam models of Fig. 9 to determine the three quantities, $\bar{\delta}_i$, $i = 1, 2, 3$. Consider first the continuous infinite beam model of Fig. 9a. For this beam $w(x) = 0$ (see Fig. 10a) and there are three geometric boundary conditions for this beam, namely that the slope at $0$ and $l = l_2/2$, or at $n \times l$ (where $n$ is any integer), is zero and the deflections at $0$ and $l$are of opposite sign. Since Eq. (B.2) is a fourth order ordinary differential equation, a fourth boundary condition is needed. This must be a force—or a moment—related condition because all the symmetry in the situation has been exploited with the geometric boundary conditions. However, it is not obvious from elementary beam theory how one might obtain the fourth condition, the one related to force - or a moment, due to the fact that the beam is infinite in length. Actually the long length of the beam is the key to the solution because the equation of three moments (Timoshenko and Young, 1945, *Theory of Structures*, McGraw Hill, New York, pp. 343.) may be used to find the moment at a point of application of the cross-link force. The moment is found to be the magnitude of $P \times l_2/2$, or $w/2$. Note from Fig. 2c that the force $P$ must be equal to $w \times l_2$. The mean deflections, which are equal, are then given by

$$\bar{\delta}_1 = \bar{\delta}_2 = \frac{5Pl_2^3}{3072EI}. \tag{B.3}$$

This result gives the deflections $\bar{\delta}_i$, $i = 1, 2$, in terms of the flexural rigidity $EI$ of the longitudinal actin filament, the force $P = w \times l_2$ that the fimbrin cross-link exerts transversely on the infinite beam, and the length $l_2$.

We also need to determine a similar formula for $\bar{\delta}_3$. To that end we consider the continuous infinite beam model of Fig. 9b. For this beam $w(x) = w$ (a constant) (see Fig. 10b) and the three geometric boundary

conditions for this beam are the same as they were for the beam in Fig. 9a. The equation of three moments again supplies the missing condition, the moment at a point of application of the force $P$. The moment is found to be equal to $w \times l_2^2/12$. The mean deflection is then given by

$$\bar{\delta}_3 = \frac{P l_2^3}{720 EI}, \tag{B.4}$$

This result gives the deflection $\bar{\delta}_3$, in terms of the flexural rigidity $EI$ of the longitudinal actin filament, the force $P = w \times l_2$ that the fimbrin cross-link exerts transversely on the infinite beam, and the length $l_2$. Substituting the results (B.3) and (B.4) into (B.1) a reduced expression for the desired $E^*$ is obtained:

$$E^* = \frac{203 EI}{l_2^4}. \tag{B.5}$$

## References


Aarden, E.M., Wassenaar, A.M., Alblas, M.J., Nijweide, P.J., 1996. Immunocytochemical demonstration of extracellular matrix proteins in isolated osteocytes. Histochemistry and Cell Biology 106, 495–501.

Almekinders, L.C., Banes, A.J., Ballenger, C.A., 1993. Effects of repetitive motion on human fibroblasts. Med. Sci. Sports. Exer. 25, 603–607.

Bretscher, A., Weber, K., 1980. Fimbrin, a new microfilament-associated protein present in microvilli and other cell surface structures. Journal of Cell Biology 86, 335–340.

Buckwalter, J.A., Rosenberg, L.C., 1982. Electron Microscopic Studies of Cartilage proteoglycans. Direct Evidence for the variable length of the chondroitin sulfate-rich region of proteoglycan subunit core protein. Journal of Biological Chemistry 257 (16), 9830–9839.

Burger, E.H., Klein-Nulend, J., 1999. Mechanotransduction in bone - role of the lacuno-canalicular network. FASEB Journal 13, S101–S112.

Burger, E.H., Veldhuijzen, J.P., 1993. Influence of mechanical factors on bone formation, resorption, and growth in vitro. In: Hall, B.K. (Ed.), Bone, Vol. 7. CRC Press, Boca Raton, Florida, pp. 37–56.

Burr, D.B., Milgrom, C., Fyhrie, D., Forwood, M., Nyska, M., Finestone, A., Hoshaw, S., Saiag, E., Simkin, A., 1996. In vivo measurement of human tibial strains during vigorous activity. Bone 18 (5), 405–410.

Chailley, B., Nicolas, G., Laine, M.C., 1989. Organization of actin microfilaments in the apical border of oviduct ciliated cells. Biology of the Cell 67, 81–90.

Cooper, R.R., Milgram, J.W., Robinson, R.A., Maryland, B., 1966. Morphology of the osteon. Journal of Bone and Joint Surgery 48-A (7), 1239–1271.

Cowin, S.C., 1999. Bone poroelasticity. Journal of Biomechanics 32 (3), 217–238.

Cowin, S.C., Moss-Salentijn, L., Moss, M.L., 1991. Candidates for the mechanosensory system in bone. Journal of Biomechanical Engineering 113 (2), 191–197.

Cowin, S.C., Weinbaum, S., Zeng, Y., 1995. A Case for Bone Canaliculi as the Anatomical Site of Strain Generated Potentials. Journal of Biomechanics 28, 1281–1297.

Curry, F.E., 1986. Determinants of capillary permeability: a review of mechanisms based on single capillary studies in the frog. Circulation Research 59 (4), 367–380.

Dupuis, D.E., Guilford, W.H., Wu, J., Warshaw, D.M., 1997. Actin filament mechanics in the laser trap. Journal of Muscle Research and Cell Motility 18, 17–30.

Fritton, S.P., Kenneth, J.M., Rubin, C.T., 2000. Quantifying the Strain History of Bone: spatial Uniformity and Self-similarity of Low Magnitude Strains. Journal of Biomechanics 33, 317–325.

Glenney Jr., J.R., Kaulfus, P., Matsudaira, P., Weber, K., 1981. F-actin binding and bundling properties of fimbrin, a major cytoskeletal protein of microvillus core filaments. Journal of Biological Chemistry 256, 9283–9288.

Gohel, A.R., Hand, A.R., Gronowicz, G.A., 1995. Immunogold localization of beta 1-integrin in bone: effect of glucocorticoids and insulin-like growth factor I on integrins and osteocyte formation. Journal of Histochemistry and Cytochemistry. 43, 1085–1096.

Guilak, F., Ratcliffe, A., Mow, V.C., 1995. Chondrocyte deformation and local tissue strain in articular cartilage: a confocal microscopy study. Journal of Orthopedic Research 13, 410–421.

Guo, P., Weinstein, A.M., Weinbaum, S., 2000. A hydrodynamic mechanosensory hypothesis for brush border microvilli. American Journal of Physiology, Renal Physiology 279, F698–F712.

Holtrop, M.E., 1975. The ultrastructure of bone. Annals of Clinical and Laboratory Science 5 (4), 264–271.

Horwitz, A.F., 1997. Integrins and Health. Scientific American 276 (5), 68–75.

Hu, X., Adamson, R.H., Liu, B., Curry, F.E., Weinbaum, S., 2000. Starling forces that oppose filtration after tissue oncotic pressure is increased. American Journal of Physiology Heart Circulation Physiololgy 279 (4), H1724–H1736.

King, G.J., Holtrop, M.E., 1975. Actin-like filaments in bone cells of cultured mouse calvaria as demonstrated by binding to heavy meromyosin. Journal of Cell Biology 66, 445–451.

Kishino, A., Yanagida, A., 1988. Force measurements by micro manipulation of a single actin filament by glass needles. Nature 334, 74–76.

Klein-Nulend, J., van der Plas, A., Semeins, C.M., Ajubi, N.E., Frangos, J.A., Nijweide, P.J., Burger, E.H., 1995. Sensitivity of osteocytes to biomechanical stress in vitro. FASEB Journal 9, 441–445.

Knothe Tate, M.L., Knothe, U., 2000. An ex vivo model to study transport processes and fluid flow in loaded bone. Journal of Biomechanics 33, 247–254.

Lanyon, L.E., Hampson, W.G.J., Goodship, A.E., Shah, J.S., 1975. Bone deformation recorded in vivo from strain gauges attached to the human tibial shaft. Acta Orthopedica Scandinavica. 46, 256–268.

Marotti, G., Cane, V., Palazzini, S., Palumbo, C., 1990. Structure-function relationships in the osteocyte. Italian Journal of Mineral & Electrolyte Metabolism 4 (2), 93–106.

Maunsbach, A.B., 1973. Ultrastructure of the proximal tubule. In: Orloff, J., Berliner, R.W. (Eds.), Handbook of Physiology. Renal Physiology. Sect. 8, American Physiological Society Washington DC, pp. 31–79 (Chapter 2).

Mooseker, M.S., Tilney, L.G., 1975. Organization of an actin filament-membrane complex. Filament Polarity and membrane attachment in the microvilli of intestinal epithelial cells. Journal of Cell Biology 67, 725–743.

Murray, D.W., Rushton, N., 1990. The effect of strain on bone cell prostaglandin E2 release: a new experimental method. Calciferous Tissue International 47, 35–39.

Nakamura, H., 1995. Localization of CD44, the hyaluronate receptor, on the plasma membrane of osteocytes and osteoclasts in rat tibiae. Cell Tissue Research 280, 225–233.

Oosawa, F., 1977. Actin-actin bond strength and the conformational change of F-actin. Biorheology 14, 11–19.

Owan, M., Triffitt, J.T., 1976. Extravascular albumin in bone tissue. Journal of Physiology 257, 293–307.

Piekarski, K., Munro, M., 1977. Transport mechanism operating between blood supply and osteocytes in long bones. Nature 269 (5623), 80–82.

Pitsillides, A.A., Rawlinson, S.C., Suswillo, R.F., Bourri, S., Zaman, G., Lanyon, L.E., 1995. Mechanical strain-induced NO production by bone cells: a possible role in adaptive bone (re)modeling? FASEB Journal 9, 1614–1622.

Reich, K.M., Frangos, J.A., 1991. Effects of flow on prostaglandin E2 (PGE2) and inositol trisphosphate (IP3) levels in osteoblasts. American Journal of Physiology 261, C428–3432.

Rubin, C.T., Lanyon, L.E., 1984. Regulation of bone formation by applied dynamic loads. Journal of Bone and Joint Surgery 66A, 397–410.

Rubin, C.T., McLeod, K.J., 1996. Inhibition of osteopenia by biophysical intervention. In: Marcus, R., Eldman, D., Kelsey, J. (Eds.), Osteoporosis. Academic Press, New York, pp. 351–371.

Salzstein, R.A., Pollack, S.R., 1987. Electromechanical potentials in cortical bone-I, experimental analysis. Journal of Biomechanics 20, 271–280.

Satcher Jr., R.L., Dewey Jr., C.F., 1996. Theoretical estimates of mechanical properties of the endothelial cell cytoskeleton. Biophysical Journal 71, 109–118.

Sauren, Y.M.H.F., Mieremet, R.H.P., Groot, C.G., Scherft, J.P., 1992. An electron microscopic study on the presence of proteoglycans on the mineralized matrix of rat and human compact lamellar bone. The Anatomical Record 232, 36–44.

Scott, G.C., Korostoff, E., 1990. Oscillatory and step response electromechanical phenomena in human and bovine bone. Journal of Biomechanics 23, 127–143.

Shapiro, F., Cahill, C., Malatantis, G., Nayak, R.C., 1995. Transmission electron microscopic demonstration of vimentin in rat osteoblast and osteocyte cell bodies and processes using the immunogold technique. Anatomical Record 241, 39–48.

Shin, D., Athanasiou, K., 1999. Cytoindentation for Obtaining Cell Biomechanical properties. Journal of Orthopaedic Research 17, 880–890.

Tanaka-Kamioka, K., Kamioka, H., Ris, H., Lim, S.S., 1998. Osteocyte shape is dependent on actin filaments and osteocyte processes are unique actin-rich projections. Journal of Bone and Mineral Research 13 (10), 1555–1568.

Wassermann, F., Yaeger, J.A., 1965. Fine structure of the osteocyte capsule and of the wall of the lacunae in bone. Zeitschrift fur Zellforschung 67, 636–652.

Weinbaum, S., 1998. 1997 Whitaker Distinguished Lecture: models to solve mysteries in biomechanics at the cellular level; a new view of fiber matrix layers. Annals of Biomedical Engineering 26 (4), 627–643.

Weinbaum, S., Cowin, S.C., Zeng, Y., 1994. A Model for the Excitation of Osteocytes by Mechanical Loading-induced Bone Fluid Shear Stresses. Journal of Biomechanics 27 (3), 339–360.

Weinger, J.M., Holtrop, M.E., 1974. An Ultrastructural study of bone cells: the occurrence of microtubules, microfilaments and tight junctions. Calciferous Tissue Research 14, 15–29.

Williams, J.L., Iannotti, J.P., Ham, A., Bleuit, J., Chen, J.H., 1994. Effects of fluid shear stress on bone cells. Biorheology. 31, 163–170.

You, J., Yellowley, C.E., Donahue, H.J., Zhang, Y., Chen, .Q., Jacobs, C.R., 2000. Substrate deformation levels associated with routine physical activity are less stimulatory to bone cells relative to loading-induced oscillatory fluid flow. Journal of Biomechanical Engineering 122, 387–393.

Zeng, Y., Cowin, S.C., Weinbaum, S., 1994. A Fiber Matrix Model for Fluid Flow and Streaming Potentials In the Canaliculi of an Osteon. Annals of Biomedical Engineering 22, 280–292.